

# Calculating transition amplitudes by variational quantum eigensolvers

Yohei Ibe,<sup>1,\*</sup> Yuya O. Nakagawa,<sup>1</sup> Takahiro Yamamoto,<sup>1</sup> Kosuke Mitarai,<sup>2,1</sup> Qi Gao,<sup>3</sup> and Takao Kobayashi<sup>3</sup>

<sup>1</sup>*QunaSys Inc., Aqua Hakusan Building 9F, 1-13-7 Hakusan, Bunkyo, Tokyo 113-0001, Japan*

<sup>2</sup>*Graduate School of Engineering Science, Osaka University,*

*1-3 Machikaneyama, Toyonaka, Osaka 560-8531, Japan*

<sup>3</sup>*Mitsubishi Chemical Corporation, Science & Innovation Center,  
1000, Kamoshida-cho, Aoba-ku, Yokohama 227-8502, Japan*

(Dated: November 12, 2021)

Variational quantum eigensolver (VQE) is an appealing candidate for the application of near-term quantum computers. A technique introduced in [Higgot *et al.*, Quantum **3**, 156 (2019)], which is named variational quantum deflation (VQD), has extended the ability of the VQE framework for finding excited states of a Hamiltonian. However, no method to evaluate transition amplitudes between the eigenstates found by the VQD without using any costly Hadamard-test-like circuit has been proposed despite its importance for computing properties of the system such as oscillator strengths of molecules. Here we propose a method to evaluate transition amplitudes between the eigenstates obtained by the VQD avoiding any Hadamard-test-like circuit. Our method relies only on the ability to estimate overlap between two states, so it does not restrict to the VQD eigenstates and applies for general situations. To support the significance of our method, we provide a comprehensive comparison of three previously proposed methods to find excited states with numerical simulation of three molecules (lithium hydride, diazene, and azobenzene) in a noiseless situation and find that the VQD method exhibits the best performance among the three methods. Finally, we demonstrate the validity of our method by calculating the oscillator strength of lithium hydride in numerical simulations with shot noise. Our results illustrate the superiority of the VQD to find excited states and widen its applicability to various quantum systems.

## I. INTRODUCTION

We are now in the era of noisy intermediate-scale quantum (NISQ) devices [1]. That is, we now have a programmable quantum device, or a NISQ device, that cannot be simulated by a classical computer using the best-known simulation algorithm [2, 3] within the run-time of the quantum device. Although the “quantum supremacy” experiment [2] has no immediate practical applications, we believe that there is a possibility that such a device outperforms existing classical algorithms in specific tasks. Various NISQ-oriented algorithms have been suggested recently [4–13], and among such, the variational quantum eigensolver (VQE) [14] is considered to be an appealing candidate for applications of near-term quantum computers.

The original VQE [14] is a method for constructing an approximate ground state of a Hamiltonian on a programmable quantum device based on the variational principle of quantum mechanics. The VQE constructs the approximate ground state by iteratively tuning a quantum circuit to minimize an energy expectation value of the generated state. Because the NISQ devices are believed to be capable of generating a wavefunction that is not classically achievable, the VQE has the potential to explore a variational space that has not been investigated before. To expand the potential application of the VQE other than for the ground state, a lot of works have extended the method to evaluate properties of excited

states of a target Hamiltonian [15–20]. Those methods generally inherit the iterative and variational feature of the VQE, i.e., they also iteratively optimize a quantum circuit concerning some cost function.

The major and perhaps popular algorithms among such extensions are the subspace-search VQE (SSVQE) [15], the multistate contracted VQE (MCVQE) [16], and the variational quantum deflation (VQD) [17]. While the SSVQE and the MCVQE can readily evaluate the transition amplitude  $|\langle\psi_1|A|\psi_2\rangle|^2$  of an observable  $A$  with respect to two approximate eigenstates  $|\psi_1\rangle$  and  $|\psi_2\rangle$  in a hardware-friendly manner (i.e., using less-costly quantum gates and circuits), the VQD, to the best of our knowledge, lacks such a method for evaluating the quantity [21]. Since the transition amplitude is related to properties of the system such as the absorption/emission spectrum of photon [22, 23], this severely limits the application range of the VQD method.

In this work, we fill this gap by providing a technique to evaluate the transition amplitude without using costly quantum circuits such as the Hadamard test [24]. Our technique is not only for the VQD, but can also be applied in a general setting where we have two orthogonal states  $|\psi_1\rangle$  and  $|\psi_2\rangle$  and a means to evaluate the overlap  $|\langle\psi_1|\psi_2\rangle|^2$ , and wish to evaluate  $|\langle\psi_1|A|\psi_2\rangle|^2$ . To support the significance of the proposed technique, we present a comprehensive comparison of the SSVQE, the MCVQE, and the VQD by conducting *noiseless* numerical simulations, where we use exact energy expectation values in the optimization routine of the parametrized circuit. In this test, we use molecular Hamiltonians of LiH and two azo compounds: diazene and azobenzene

\* ibe@qunasys.com

(AB). We find that, under this setting, the VQD generally exhibits better performance than the other two, which convinces the importance of our proposed technique. Finally, as a demonstration of the technique, we conduct a proof-of-principle numerical simulation of the method using a sampling simulator, i.e., expectation values of observables are simulated with the *shot noise*.

## II. EVALUATION OF TRANSITION AMPLITUDES

First, we propose a method to evaluate the transition amplitude of Hermitian operators between two quantum states. More concretely, we present how to evaluate  $|\langle\psi_1|A|\psi_2\rangle|^2$  for a Hermitian operator  $A$  and quantum

states  $|\psi_1\rangle$  and  $|\psi_2\rangle$  such that  $\langle\psi_1|\psi_2\rangle = 0$  and

$$A = \sum_i a_i P_i, \quad (1)$$

where  $P_i \in \{I, X, Y, Z\}^{\otimes n}$  and  $a_i \in \mathbb{R}$ .  $I, X, Y$ , and  $Z$  are Pauli operators. We assume that, for any given two states  $|\psi_1\rangle$  and  $|\psi_2\rangle$ , we can evaluate the overlap  $|\langle\psi_1|\psi_2\rangle|^2$ . This evaluation can be performed by, e.g., the so-called swap test [25]. Note that the requirements on the hardware of quantum computers to evaluate the overlap can be relaxed when we know quantum circuits  $U_1$  and  $U_2$  that generates  $|\psi_1\rangle$  and  $|\psi_2\rangle$ , that is, we can evaluate the overlap by  $|\langle\psi_1|\psi_2\rangle|^2 = |\langle 0|U_1^\dagger U_2|0\rangle|^2$ . This is the case for calculating the transition amplitude for approximate eigenstates obtained by the VQD.

Let us consider unitary gates

$$U_{ij,\pm} = \frac{1}{\sqrt{2}}(I \pm iP_i) \frac{1}{\sqrt{2}}(I \pm iP_j), \quad (2)$$

which can be realized as a product of Pauli rotation gates  $U_{ij,\pm} = e^{\pm i\frac{\pi}{4}P_i} e^{\pm i\frac{\pi}{4}P_j}$ . We can show the following equality holds under the assumption of  $\langle\psi_1|\psi_2\rangle = 0$ ,

$$\begin{aligned} |\langle\psi_1|A|\psi_2\rangle|^2 &= \sum_i a_i^2 |\langle\psi_1|P_i|\psi_2\rangle|^2 \\ &+ \sum_{i < j} a_i a_j \left[ 2|\langle\psi_1|U_{ij,+}|\psi_2\rangle|^2 + 2|\langle\psi_1|U_{ij,-}|\psi_2\rangle|^2 - |\langle\psi_1|P_i|\psi_2\rangle|^2 - |\langle\psi_1|P_j|\psi_2\rangle|^2 - |\langle\psi_1|P_i P_j|\psi_2\rangle|^2 \right], \end{aligned} \quad (3)$$

which can be employed to evaluate  $|\langle\psi_1|A|\psi_2\rangle|^2$ . More concretely, we can measure each term in the right-hand side of Eq. (3) on a quantum device by regarding it as a overlap between two states because  $P_i, P_j, U_{ij,\pm}$  are unitary and  $P_i|\psi\rangle, P_j|\psi\rangle, U_{ij,\pm}|\psi\rangle$  can be realized on the device. We then combine the results of measurement according to the equation. Note that the assumption  $\langle\psi_1|\psi_2\rangle = 0$  should always be satisfied.

Equation (3) is one of the main results of this work. It reduces the evaluation of the transition amplitudes to a sequence of measurements of overlaps of two states. On the other hand, if we allow more complicated circuits to be executed on a device, we can construct an ancilla based technique to evaluate  $\langle\psi_1|A|\psi_2\rangle$  as shown in Appendix B.

## III. COMPARISON OF ALGORITHMS FOR EXCITED STATES

In this section, we compare the accuracy and capability of three algorithms for obtaining excited states of a given Hamiltonian on near-term quantum computers, namely

the SSVQE, the MCVQE, and the VQD, by noiseless numerical simulations. By “noiseless”, we mean all of the expectation values required in the algorithms are exactly computed. This situation is ideal compared with the real NISQ devices but still appropriate for discerning the capability of the algorithms. This section aims to support the significance of our method proposed in the previous section by showing that the VQD gives the best performance among the three.

For the comparison, we use electronic Hamiltonians of LiH, diazene, and AB molecule. LiH is considered and employed as a simple “benchmark” molecule by a variety of studies on quantum computational chemistry [26–29]. Diazene and AB, on the other hand, are more relevant to applications of quantum chemistry to industry. In particular, AB is one of the most representative organic molecules which show cis-trans photoisomerization in photochemistry. AB has been attracting significant interests from the viewpoints of its photo-physics/photochemistry associated with its various applications of photo-functional materials, and its derivatives are widely used as important photo-functional dyes in the industry [30]. For photo-functional molecules such

as AB and its derivatives, it is crucial to theoretically predict their photophysical properties such as absorption/emission spectra or emission quantum yields and to elucidate their photochemical reaction mechanisms. Although the elucidation of its photoisomerization mechanism has been made theoretically so far, it remains controversial whether it proceeds with rotation or inversion or others. The simulations presented here do not only support the significance of the proposed method, but can also be viewed as a first step toward the real-world application of NISQ devices.

### A. Settings of numerical simulation

Here we describe setups of numerical simulations for comparing the SSVQE, the MCVQE, and the VQD (the details of three algorithms are explained in Appendix A). As a variational quantum circuit for trial wavefunctions, we adopt an ansatz shown in Fig. 1 for all three algorithms. We call this ansatz real-valued symmetry-preserving (RSP) ansatz,  $U_{\text{RSP}}(\theta)$ , where  $\theta$  are classical parameters to be optimized. It is a slightly modified version of a heuristic ansatz introduced in Ref. [31], which preserves the number of particles of a reference state, so that the generated wavefunction is always a real-valued vector in the computational basis. As reference states for trial wavefunctions, we use the spin-restricted closed-shell Hartree-Fock state and singly excited states. The BFGS method [32] is employed for classical optimization of the ansatz quantum circuit. The convergence criterion is set so that the optimization terminates when the relative difference of energy expectation value between iterations becomes lower than  $10^{-8}$ . The electronic Hamiltonian is computed by PySCF [33], an open-source quantum chemistry library, and mapped to the qubit Hamiltonian by the Jordan-Wigner transformation [34]. Note that the RSP ansatz only works for the Jordan-Wigner transformation. For all simulations in this section, the weight vector for the SSVQE (see Appendix A 2) is set as  $w = (k, k-1, \dots, 1)$ , where  $k$  is the number of quantum states to be calculated.

In the simulations, we compute several singlet and triplet eigenstates in the low-energy spectrum of the electronic Hamiltonians of LiH, diazene, and AB. To circumvent the need to find all three degenerate eigenstates in each triplet subspace, we slightly modify the original electronic Hamiltonian  $H$  to

$$H' = H + \alpha S_z^2, \quad (4)$$

where  $S_z$  is an operator representing the  $z$ -component of the total electron spin, and  $\alpha > 0$ . When  $\alpha$  is sufficiently large, all eigenstates of  $H$  which have non-zero  $S_z$  are projected out from the low-energy subspace of  $H'$ . In the following subsections, we use this  $H'$  with  $\alpha = 4$  in atomic units as the target Hamiltonian in the optimization process presented above. This approach of adding “penalty terms” to a Hamiltonian can be found in Ref.

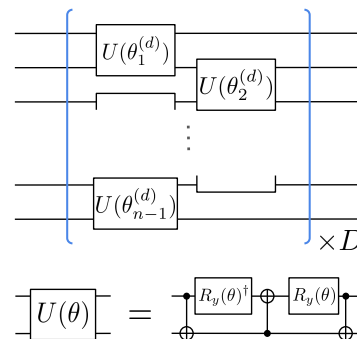


FIG. 1. Real-valued symmetry-preserving (RSP) ansatz. In the figure,  $R_y(\theta) = \exp(-i\theta Y/2)$ . The rotation angles implemented in two-qubit unitary gates  $U(\theta)$  are parameters to be optimized.  $D$  denotes the depth of the circuit.

[35]. All simulations in this section are performed using Qulacs [36].

### B. Simple benchmark molecule: LiH

As for LiH molecule, we take STO-3G minimal basis set and all molecular orbitals into consideration, resulting in the number of simulated qubits being 12. The RSP ansatz mentioned above with  $D = 10$  is used as the variational quantum circuit, where the total number of parameters is 110. We calculate three energy levels  $S_0$ ,  $T_1$ , and  $S_1$  for 36 points of the interatomic length of LiH and compared with the full configuration interaction (full-CI) calculations. As the initial values of ansatz parameters  $\theta$ , we use uniform random numbers drawn from  $[0, 2\pi]$  for the first point of the potential energy curve (PEC), and after that, we employ the optimized parameters of an adjacent point of the PEC.

Calculated energies and their errors of LiH molecule by the SSVQE, the MCVQE, and the VQD are shown in Fig. 2 along with the result of the full-CI calculations. As seen in Fig. 2 (bottom), the VQD (the green lines) gives the most accurate energies than the other two, keeping the “chemical accuracy” throughout the plot.

### C. More complex systems: diazene and azobenzene

#### 1. Diazene

For diazene, we present VQE simulations using molecular structures along its minimum energy path (MEP) between trans and cis isomers. First, we obtain the structures by MEP calculations using the state-averaged complete active space self-consistent field (SA-CASSCF) method implemented in Molpro 2015 [37] with the 6-31G\* basis set. The MEP calculations are done with the Gonzalez-Schlegel method [38]. We use an active space

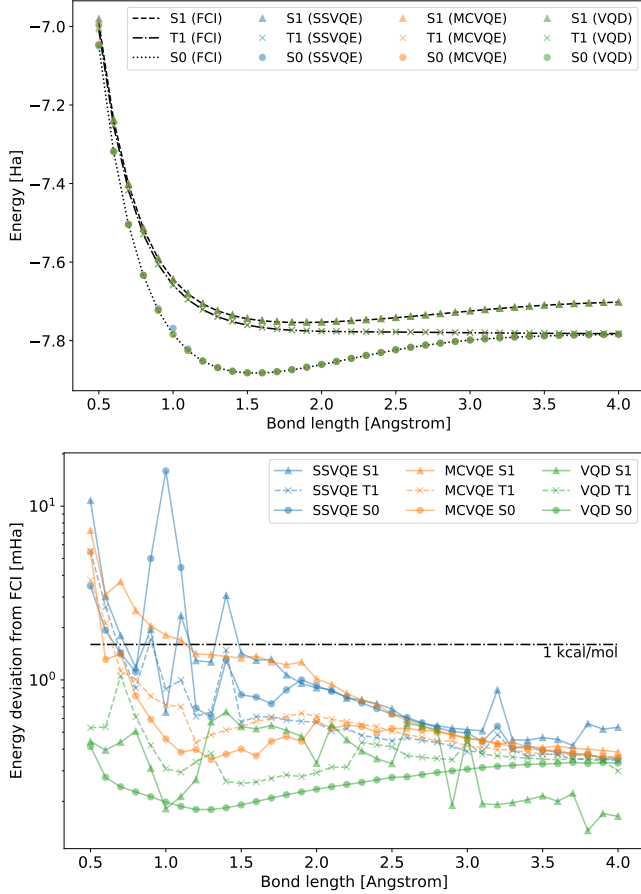


FIG. 2. Simulation of LiH molecule by the SSVQE, the MCVQE, and the VQD. (top) The potential energy curve. Most of data points for three algorithms are overlapped. (bottom) Energy deviations from the full-CI (FCI) calculations. The horizontal dashed line denotes the “chemical accuracy”.

consisting of 4 orbitals ( $2 \times (\text{lone pair on N}) + \pi (\text{HOMO}) + \pi^* (\text{LUMO})$ ) with 6 electrons. The  $S_0$ - $S_3$  and  $T_1$ - $T_3$  states are averaged in the SA-CASSCF calculations. In the simulations, we use several points on  $S_2$  MEP, from  $S_2$  Franck-Condon (FC) state of trans/cis isomers to the  $S_2$  minimum, which proceeds with a rotation about the N-N bond associating the disruption of the double bond. Then, we perform the SSVQE, the MCVQE, and the VQD simulations of the Hamiltonians constructed in the same active space along the MEP and compare them with complete active space configuration interaction (CASSCF) calculations, i.e., energies obtained by the exact diagonalization within the active space. The number of qubits to be simulated is eight. Here we utilize the RSP ansatz mentioned above with  $D = 20$ , where the total number of parameters is 140. Again, the initial values of ansatz parameters are taken as uniform random numbers drawn from  $[0, 2\pi]$  for the first point on the MEP. For other points on the MEP, optimized parameters at an adjacent point are used as initial values of parameters.

In addition to the energy of each eigenstate, we also

calculate oscillator strength  $f_{ij}$  between each pair of spin-singlet states  $|S_i\rangle$  and  $|S_j\rangle$ . It is defined as

$$f_{ij} = \frac{2}{3}(E(S_j) - E(S_i)) \sum_{\alpha=x,y,z} |\langle S_j | R_\alpha | S_i \rangle|^2, \quad (5)$$

where  $E(S)$  is the energy of  $|S\rangle$ ,  $R_\alpha = \sum_{l=1}^N r_{l,\alpha}$  is the electric dipole moment operator, and  $r_{l,\alpha}$  is the  $\alpha$ -coordinate of the  $l$ -th electron. The oscillator strength gives the normalized strength of the absorption/emission spectrum of molecules [23], so it is fundamental for studying photochemical dynamics and reactions of molecules in quantum chemistry. Note that the oscillator strength involves the transition amplitude of  $R_\alpha$  operator, so it is impossible to evaluate it by the VQD on a quantum device in a hardware-friendly manner without using our proposed method in Sec. II. In this subsection, we evaluate it by exact values since we know all components of wavefunctions  $|S_i\rangle$ ,  $|S_j\rangle$  and the matrix elements of  $R_\alpha$  by virtue of numerical simulations.

Results for diazene along the MEP are shown in Fig. 3. Calculated energies and deviations from the exact ones (Fig. 3 (a-f)) show that the VQD method gives more accurate results than the other two in our simulation settings. Moreover, from Fig. 3 (g, h, i), the VQD gives the most accurate oscillator strengths, which indicates that the method enables precise calculations of the wavefunctions as well as the energy spectrum.

## 2. Azobenzene

For AB, we perform VQE simulations using two structures: trans/cis isomers. First, we obtain optimized trans/cis isomers using SA-CASSCF calculations, using an active space consisting of 3 orbitals ( $(\text{lone pair on N}) + \pi (\text{HOMO}) + \pi^* (\text{LUMO})$ ) with 4 electrons. The  $S_0$ - $S_4$  and  $T_1$ - $T_3$  states are averaged in the SA-CASSCF calculations. The structures used in the VQE simulations are the minimum energy structures of  $S_0$  state. Then, we perform the VQE simulations for the Hamiltonian in the same active space to obtain the eigenenergies and their deviations from the exact energies obtained by the exact diagonalization of the Hamiltonian. In this case, the number of qubits is six and we utilize RSP ansatz with  $D = 10$ , where the total number of parameters is 50. The oscillator strength is calculated as well by using the converged states. As the initial values of ansatz parameters, we use uniform random numbers within  $[0, 2\pi]$ .

Results are shown in Fig. 4. Inheriting the trend from the previous results, the VQD gives more accurate results than the other two. Moreover, as evident in Fig. 4 (g, h, i), the VQD gives the most accurate oscillator strengths, which indicates that the method enables us to generate precise wavefunctions.

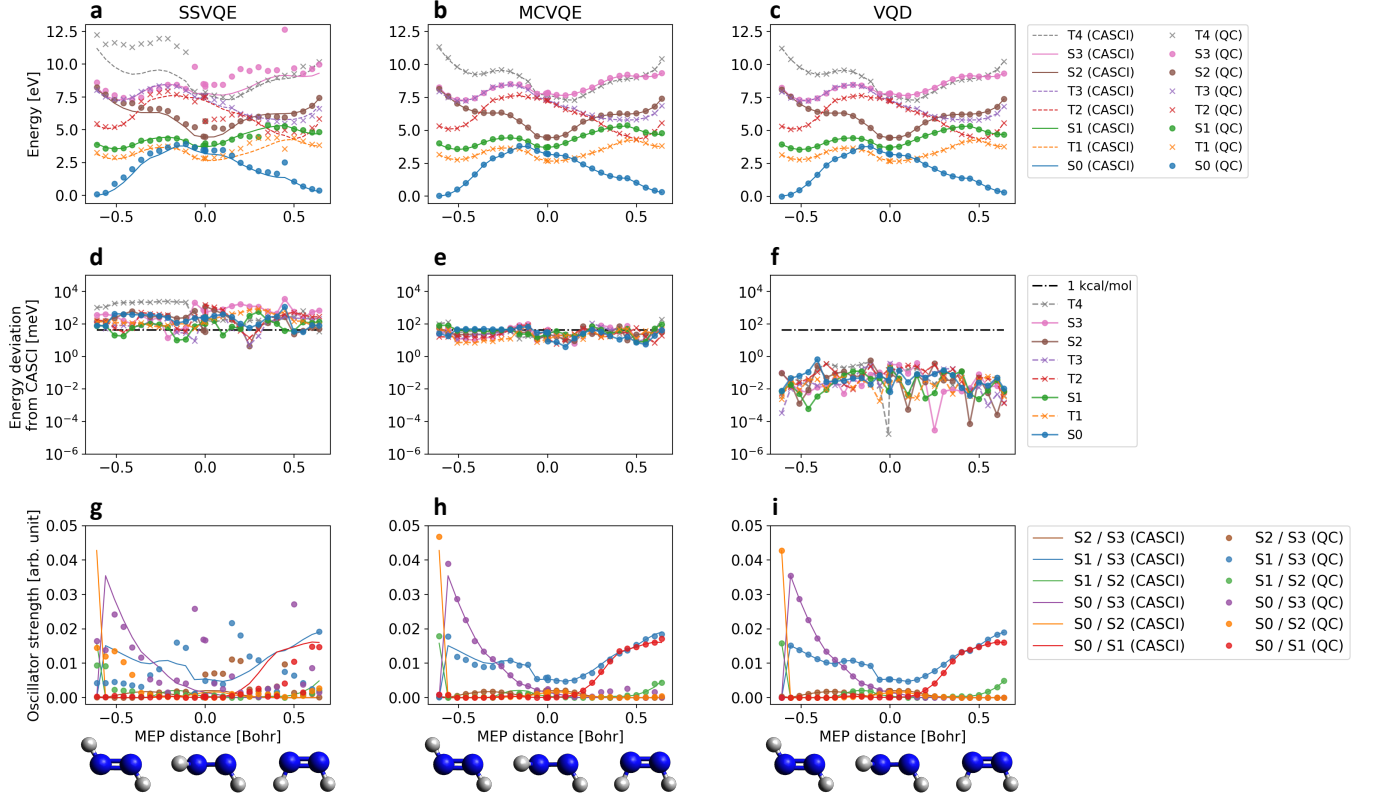


FIG. 3. Potential energy curves along an  $S_2$  MEP, from trans to cis structure of diazene calculated by (a) SSVQE, (b) MCVQE, and (c) VQD. Here, we set trans- $S_0$  minimum as zero energy, and the units of the MEP distance are mass-weighted coordinates divided with the square root of the total mass of the molecule. (d), (e), (f): The energy deviations of each method from the exact CASCI calculations. The dashed horizontal line denotes the “chemical accuracy”. (g), (h), (i): Oscillator strength between each pair of singlet states calculated by respective methods. Several atomic structures on the MEP are displayed at the bottom of the figure.

#### D. Discussion

We have observed that the VQD has a better performance compared to the SSVQE and the MCVQE in this section. This result is probably because the requirement for the ansatz quantum circuit  $U(\theta)$  is looser for the VQD than the SSVQE and the MCVQE; the ansatz with optimal parameters must make all reference states reside in the low-energy subspace *simultaneously* in the SSVQE and the MCVQE, while the VQD can do it *separately* for each reference state by the ansatz with different optimized parameters.

Moreover, the performance of the SSVQE seems worse than the MCVQE in our simulations. The part of the reason is because we employ the “weighted-sum” version of the SSVQE in the simulation [15]. If one used the “equal-weight” version of the SSVQE, which is equivalent to the MCVQE, the difference will vanish as long as the optimization of the ansatz quantum circuit goes well.

#### IV. IMPLEMENTATION OF TRANSITION AMPLITUDE EVALUATION FOR VQD

The previous section demonstrates the significance of the technique presented in Sec. II. That is, we provide the hardware-friendly way to evaluate the transition amplitude between two eigenstates with the most accurate method for generating excited states among the previously proposed three methods. In this section, to verify the correctness of the technique, we run it on a more realistic simulator that contains noise in expectation values of observables.

We employ the molecular Hamiltonian of LiH and take the active space of (2e, 2o) with STO-3G minimal basis set. We run the VQD simulation to calculate the potential energy curves of two singlet states,  $S_0$  and  $S_1$ , and calculate the oscillator strength between them by the method in Sec. II. We take 36 points of the bond distances from 0.5 to 4.0 Å. The parity-mapping [39] is used to map a fermionic (electron) Hamiltonian to a qubit Hamiltonian and to reduce the number of qubits from 4 to 2 utilizing the symmetry of particle number and  $S_z$  [40]. As the ansatz for the VQD, we use the “RY ansatz” of

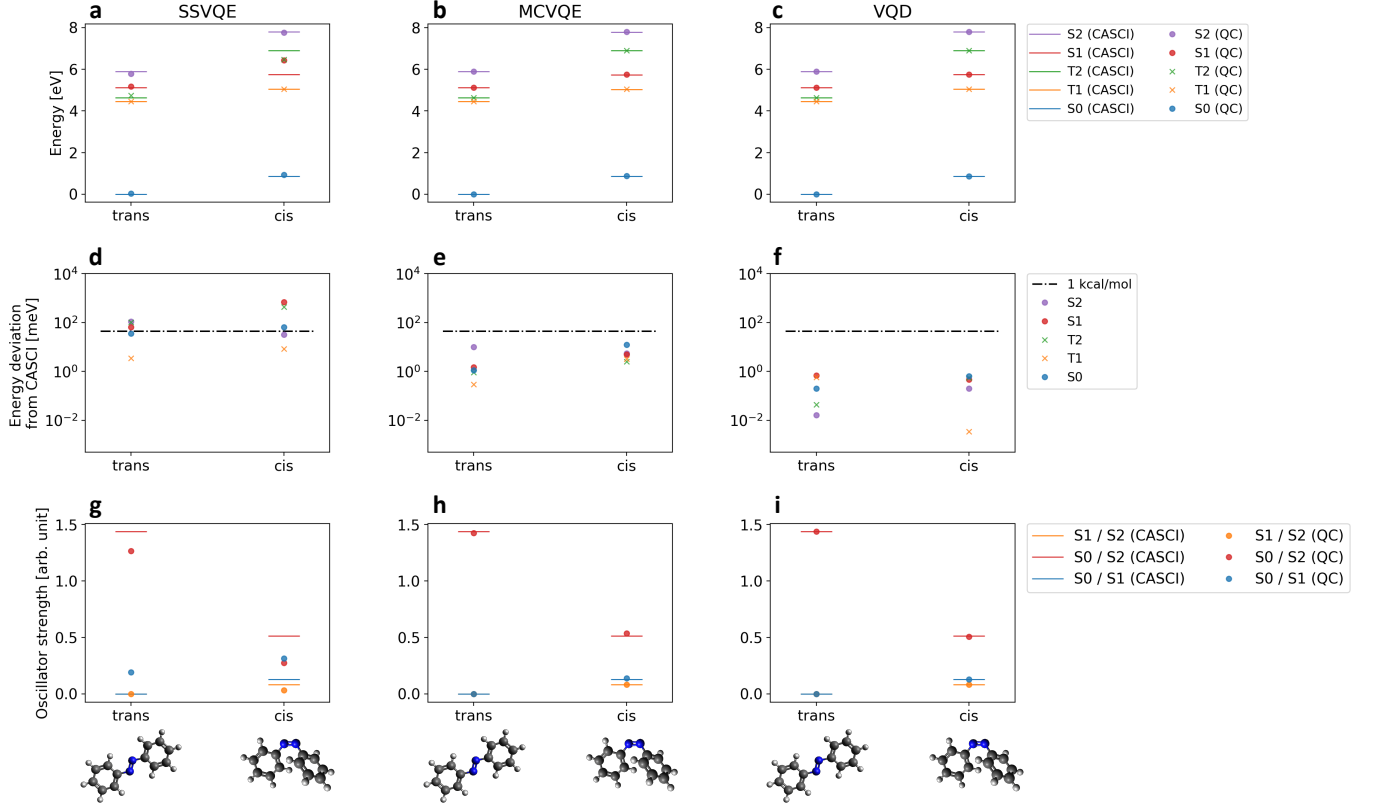


FIG. 4. Energy levels of trans/cis AB calculated by (a) SSVQE, (b) MCVQE, and (c) VQD, where we set trans- $S_0$  state as zero energy. (d), (e), (f): The energy deviations of each method from the exact CASCI calculations. Dashed horizontal line denotes the “chemical accuracy”. (g), (h), (i): Oscillator strength between each pair of singlet states calculated by respective methods. The atomic structures are presented at the bottom of the figure.

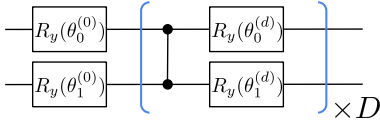


FIG. 5. RY ansatz. The rotation angles in  $R_y(\theta) = \exp(-i\theta Y/2)$  are parameters to be optimized.  $D$  denotes the depth of the circuit.

depth= 2, which is available in Qiskit Aqua v0.6.4 [41] as `qiskit.aqua.components.variational_forms.RY` (see Fig. 5). For classical minimization of the cost function, the SLSQP method [32] is employed. Similar to the previous section, we set the convergence criterion so that the optimization terminates when the relative difference of energy expectation value between iterations becomes lower than  $10^{-8}$ . Energy derivatives concerning the circuit parameters are calculated with the so-called parameter-shift rule [42, 43] to mitigate the shot noise explained in the next paragraph. To obtain only spin-singlet states, we add the expectation value of the total spin  $\langle S^2 \rangle$  as a penalty term to the cost function of the

VQD. The simulation in this section is performed using Qiskit [41].

We test two options on simulating energy expectation values and overlaps in the optimization routine of the VQD: using an exact noiseless simulator or using a noisy sampling simulator. The former simulator is the same as explained in the previous section. In the latter, the expectation value of the energy is obtained by sampling  $10^5$  shots for each Pauli term in the Hamiltonian throughout the simulation. This sampling introduces the fluctuation in the energy expectation values, i.e., shot noise. Similarly, for evaluating overlaps like  $|\langle 0|U_1^\dagger U_2|0\rangle|^2$ ,  $10^5$  shots measurements are sampled. In both cases, after the optimization in the VQD, we calculate the oscillator strength by the sampling simulator, which brings the shot noise, by our method in Sec. II.

In Fig. 6, we show the result of the simulation. When using the sampling simulator in the whole process (blue dots in Fig. 6), calculated energies almost achieve the exact solution; however, oscillator strengths deviate from the exact values at large bond lengths, because of the imperfection of the optimizations coming from the shot noise. On the other hand, under the accurately optimized parameters without the shot noise (orange dots in Fig. 6),



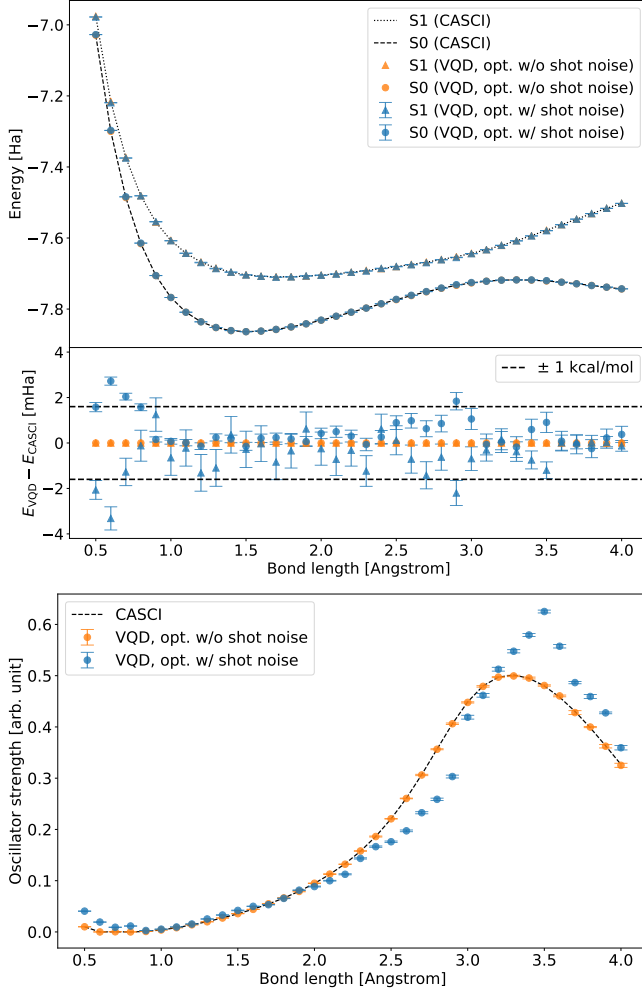


FIG. 6. Numerical simulation of LiH (2e, 2o) using the VQD. (top) Potential energy curve of  $S_0$  and  $S_1$  states and its deviation from exact CASCI calculations. (bottom) Oscillator strength between  $S_0$  and  $S_1$  states. For the VQD calculations, “opt. w/ (w/o) shot noise” indicates that the numerical simulation optimizes the circuit parameters with (without) the shot noise. In both cases, we calculate oscillator strengths *with* the shot noise after the optimization. Error bars are calculated in a way explained in Appendix C.

the VQD almost perfectly reproduces the exact oscillator strengths. These results illustrate the correctness of our method in calculating oscillator strengths.

## V. CONCLUSION

In this work, we propose a general technique to evaluate transition amplitudes between two orthogonal states in a hardware-friendly manner on a quantum device. Its immediate application is the evaluation of transition amplitudes between the approximate eigenstates of the Hamiltonian obtained by the VQD method. The significance of the proposed method is supported by the com-

prehensive comparison of the three method, namely the SSVQE, the MCVQE and the VQD, in noiseless simulations which show the advantage of using the VQD for generating approximate excited states. Finally, we also verifies the correctness of the proposed method by running it in a more realistic situation for near-term computers. This work enlarges the possibility of the VQD and greatly advances the field of excited states calculations on a quantum device.

## ACKNOWLEDGEMENT

This work was supported as part of a joint development agreement between Mitsubishi Chemical Corporation and QunaSys. A part of the numerical simulations in this work was done on Microsoft Azure Virtual Machines provided through the program Microsoft for Startups. YI, YON, TY, and KM acknowledge Wataru Mizukami and Tennin Yan for valuable discussions.

## Appendix A: Review of algorithms

In this section, we provide a review of the algorithms used in the main text.

### 1. VQE

The VQE [14] is a variational algorithm for finding the ground state of a system of  $n$ -qubits whose Hamiltonian is in the form of

$$H = \sum_{P \in \{I, X, Y, Z\}^{\otimes n}} h_P P. \quad (\text{A1})$$

where  $I, X, Y, Z$  are single-qubit Pauli operators and  $h_P \in \mathbb{R}$  is a coefficient. If the number of terms with  $h_P \neq 0$  in the summation is not too large, we can evaluate the expectation value of the Hamiltonian, or energy of the system, by evaluating expectation values of each  $P$  and then summing them on a classical computer. To approximate the ground state of the Hamiltonian, the VQE uses parameterized quantum circuit  $U(\theta)$ , and iteratively optimize the parameter  $\theta$  so that the energy expectation value  $E(\theta) := \langle 0 | U^\dagger(\theta) H U(\theta) | 0 \rangle$ , where  $|0\rangle$  is an initialized state of the quantum computer, is minimized. The VQE algorithm proceeds as follows:

1. Define a quantum circuit  $U(\theta)$  with parameters  $\theta$ .
2. Repeat the followings until the convergence of  $E(\theta)$ .
  - (a) Generate a state  $|\psi(\theta)\rangle := U(\theta) |0\rangle$ .
  - (b) Evaluate the energy  $E(\theta)$  by measuring  $\langle 0 | U^\dagger(\theta) H U(\theta) | 0 \rangle$ .
  - (c) Update the parameter  $\theta$  to decrease  $E(\theta)$ .

When the convergence is reached, we expect that  $|\psi(\boldsymbol{\theta})\rangle$  and  $E(\boldsymbol{\theta})$  is an approximate ground state and its energy from the variational principle of the quantum mechanics.

## 2. Subspace-search VQE

The SSVQE [15] uses multiple initial states to search low-energy subspace of a Hamiltonian. The SSVQE algorithm can be summarized as follows:

1. Define an ansatz quantum circuit  $U(\boldsymbol{\theta})$  and mutually orthogonal initial states (reference states)  $\{|\varphi_i\rangle\}_{i=1}^k$ . The reference states must be chosen so that one can readily make superpositions of them on a quantum device such as the computational basis.
2. Repeat the following steps until the convergence.
  - (a) Generate a set of states  $|\psi_i(\boldsymbol{\theta})\rangle := U(\boldsymbol{\theta})|\varphi_i\rangle$ .
  - (b) Evaluate a cost function defined as a weighted sum of energies,  $L_{\mathbf{w}}(\boldsymbol{\theta}) := \sum_{i=1}^k w_i \langle \psi_i(\boldsymbol{\theta}) | H | \psi_i(\boldsymbol{\theta}) \rangle$ , where the weight vector  $\mathbf{w}$  is chosen such that  $w_1 > w_2 > \dots > w_k > 0$ .
  - (c) Update parameter  $\boldsymbol{\theta}$  to decrease  $L$ .

The weight vector  $\mathbf{w}$  has the effect of choosing which  $|\varphi_i\rangle$  converges to which excited state. The cost function  $L_{\mathbf{w}}(\boldsymbol{\theta})$  reaches its global minimum when the ansatz circuit  $U(\boldsymbol{\theta})$  maps  $|\varphi_i\rangle$  to the  $i$ -th excited state  $|E_i\rangle$  of the Hamiltonian.

We note here that the assumed ability to create the superposition of  $\{|\varphi_i\rangle\}_i$  enables us to evaluate transition amplitudes of an operator between two eigenstates. It can be performed by creating two different superpositions of two eigenstates, measuring the operator of the interest, and postprocessing on a classical computer [15].

## 3. Multistate contracted VQE

The protocol of MCVQE [16] is similar to that of the SSVQE. It works as follows:

1. Perform Step 1 and 2 of the SSVQE, using a cost function where the weight vector is omitted:  $L(\boldsymbol{\theta}) := \sum_{i=1}^k \langle \psi_i(\boldsymbol{\theta}) | H | \psi_i(\boldsymbol{\theta}) \rangle$ .
2. Using the converged  $\boldsymbol{\theta}^*$ , evaluate  $\tilde{H}_{ij} := \langle \psi_i(\boldsymbol{\theta}) | H | \psi_j(\boldsymbol{\theta}) \rangle$  for all  $i$  and  $j$ .
3. Diagonalize the matrix  $\tilde{H} = \{\tilde{H}_{ij}\}_{i,j=1}^k$  on a classical computer.

Energy spectrum of  $\tilde{H}$  approximates that of the original  $H$ , and approximate eigenstates are obtained by superposing  $\{|\psi_i(\boldsymbol{\theta})\rangle\}_i$  with coefficients determined by the

eigenvectors of  $\tilde{H}$ . The evaluation of transition amplitudes between the approximate eigenstates can be performed in the same manner as the SSVQE.

## 4. Variational quantum deflation

The VQD algorithm [17] is probably the most straightforward way to construct approximate eigenstates of a Hamiltonian  $H$ . The algorithm for finding the  $k$ -th excited state is as follows.

1. Perform the VQE and obtain an optimal parameter  $\boldsymbol{\theta}_0^*$  an approximate ground state  $|\psi(\boldsymbol{\theta}_0^*)\rangle$ .
2. Set  $j = 1$  and repeat the following until  $j = k$ .
  - (a) Define a Hamiltonian
 
$$H_j := H + \sum_{i=0}^{j-1} \beta_i |\psi(\boldsymbol{\theta}_i^*)\rangle \langle \psi(\boldsymbol{\theta}_i^*)|, \quad (\text{A2})$$
 where  $\{\beta_i\}$  is a set of sufficiently large real-valued coefficient.
  - (b) Perform the VQE to find an approximate ground state of  $H_j$ .
  - (c) Increment  $j$ .

The above algorithm works because  $H_j$  has the  $j$ -th excited state of the original  $H$ . To evaluate the expectation value of  $H_j$ , we need to evaluate the overlap between two states  $|\psi(\boldsymbol{\theta})\rangle$  and  $|\psi(\boldsymbol{\theta}')\rangle$ . It is suggested in [17] that we can either employ so-called destructive swap test [44] or measure them by  $|\langle 0 | U^\dagger(\boldsymbol{\theta}) U(\boldsymbol{\theta}') | 0 \rangle|^2$  exploiting the knowledge of the circuit.

We note that, while the previous two methods, namely the SSVQE and the MCVQE, can measure the transition amplitudes by creating the superposition of the initial states, there has been no efficient method for the VQD.

## Appendix B: Ancilla-based transition amplitude evaluation

Here, we describe a method to evaluate  $\langle \psi_1 | A | \psi_2 \rangle$  using an ancilla qubit. We assume that we have descriptions of circuits  $U_1$  and  $U_2$  which generates  $|\psi_1\rangle$  and  $|\psi_2\rangle$  respectively from the initialized state  $|0\rangle$ . Let,

$$\bar{\Lambda}(U_1) = |0\rangle \langle 0| \otimes U_1 + |1\rangle \langle 1| \otimes I, \quad (\text{B1})$$

$$\Lambda(U_2) = |0\rangle \langle 0| \otimes I + |1\rangle \langle 1| \otimes U_2. \quad (\text{B2})$$

Then, we have the following equality,

$$\begin{aligned} \text{Re}[\langle \psi_1 | P_i | \psi_2 \rangle] &= \\ (\langle + | \otimes \langle 0 |) \bar{\Lambda}(U_1)^\dagger \Lambda(U_2)^\dagger (X \otimes P_i) \Lambda(U_2) \bar{\Lambda}(U_1) (| + \rangle \otimes | 0 \rangle) \\ \text{Im}[\langle \psi_1 | P_i | \psi_2 \rangle] &= \\ (\langle + | \otimes \langle 0 |) \bar{\Lambda}(U_1)^\dagger \Lambda(U_2)^\dagger (Y \otimes P_i) \Lambda(U_2) \bar{\Lambda}(U_1) (| + \rangle \otimes | 0 \rangle) \end{aligned} \quad (\text{B3})$$



We can recover  $\langle \psi_1 | A | \psi_2 \rangle$  by combining them according to  $\langle \psi_1 | A | \psi_2 \rangle = \sum_i a_i \langle \psi_1 | P_i | \psi_2 \rangle$ . However, the above method uses expensive controlled- $U$  gates, which might make it unfeasible on a near-term device.

### Appendix C: Statistical errors in shot noise simulator

The error bars of the energy of the  $S_0$  and  $S_1$  states in the top panel of Fig. 6 are drawn by the outputs of `evaluate_with_result` method of `qiskit.aqua.operators.weighted_pauli_operator` of Qiskit v0.14 [41]. The output is calculated as follows.

For a Hamiltonian  $H = \sum_{i=1}^N c_i P_i$  with  $P_i$  being Pauli operator, its statistical sampling error is calculated by  $\Delta H = \sqrt{\frac{1}{N} \sum_{i=1}^N c_i^2 (\Delta P_i)^2}$ , where  $(\Delta P_i)^2$  is the variance of measurement outcome of  $P_i (= \pm 1)$ .

The error bars for the oscillator strength (bottom panel of Fig. 6), on the other hand, are calculated by propagation of the error for energies of  $S_0$  and  $S_1$  states described in the above and error in transition amplitude  $|\langle S_0 | R_\alpha | S_1 \rangle|^2$ , according to the definition of the oscillator strength (Eq. (5)). The latter error is estimated by five realized values of the transition amplitude obtained by using Eq. (3), where each term in the right-hand side is computed as  $|\langle 0 | U | 0 \rangle|^2$  (return probability of  $|0\rangle$  state after some circuit  $U$ ) with  $10^5$  shots.

- 
- [1] J. Preskill, Quantum **2**, 79 (2018).
  - [2] F. Arute, K. Arya, R. Babbush, D. Bacon, J. C. Bardin, R. Barends, R. Biswas, S. Boixo, F. G. S. L. Brandao, D. A. Buell, B. Burkett, Y. Chen, Z. Chen, B. Chiaro, R. Collins, W. Courtney, A. Dunsworth, E. Farhi, B. Foxen, A. Fowler, C. Gidney, M. Giustina, R. Graff, K. Guerin, S. Habegger, M. P. Harrigan, M. J. Hartmann, A. Ho, M. Hoffmann, T. Huang, T. S. Humble, S. V. Isakov, E. Jeffrey, Z. Jiang, D. Kafri, K. Kechedzhi, J. Kelly, P. V. Klimov, S. Knysh, A. Korotkov, F. Kostrietsa, D. Landhuis, M. Lindmark, E. Lucero, D. Lyakh, S. Mandrà, J. R. McClean, M. McEwen, A. Megrant, X. Mi, K. Michielsen, M. Mohseni, J. Mutus, O. Naaman, M. Neeley, C. Neill, M. Y. Niu, E. Ostby, A. Petukhov, J. C. Platt, C. Quintana, E. G. Rieffel, P. Roushan, N. C. Rubin, D. Sank, K. J. Satzinger, V. Smelyanskiy, K. J. Sung, M. D. Trevithick, A. Vainsencher, B. Villalonga, T. White, Z. J. Yao, P. Yeh, A. Zalcman, H. Neven, and J. M. Martinis, Nature **574**, 505 (2019).
  - [3] E. Pednault, J. A. Gunnels, G. Nannicini, L. Horesh, and R. Wisnieff, Leveraging secondary storage to simulate deep 54-qubit sycamore circuits (2019), arXiv:1910.09534.
  - [4] E. Farhi, J. Goldstone, and S. Gutmann, arXiv preprint arXiv:1411.4028 (2014).
  - [5] K. Mitarai, M. Negoro, M. Kitagawa, and K. Fujii, Phys. Rev. A **98**, 032309 (2018).
  - [6] E. Farhi and H. Neven, arXiv:1802.06002 (2018).
  - [7] V. Havlíček, A. D. Córcoles, K. Temme, A. W. Harrow, A. Kandala, J. M. Chow, and J. M. Gambetta, Nature **567**, 209 (2019).
  - [8] T. Kusumoto, K. Mitarai, K. Fujii, M. Kitagawa, and M. Negoro, arXiv:1911.12021 (2019).
  - [9] S. McArdle, S. Endo, A. Aspuru-Guzik, S. Benjamin, and X. Yuan, arXiv:1808.10402 (2018).
  - [10] Y. Cao, J. Romero, J. P. Olson, M. Degroote, P. D. Johnson, M. Kieferová, I. D. Kivlichan, T. Menke, B. Peropadre, N. P. D. Sawaya, S. Sim, L. Veis, and A. Aspuru-Guzik, Chemical Reviews **119**, 10856 (2019).
  - [11] X. Xu, J. Sun, S. Endo, Y. Li, S. C. Benjamin, and X. Yuan, arXiv preprint arXiv:1909.03898 (2019).
  - [12] H.-Y. Huang, K. Bharti, and P. Rebentrost, arXiv preprint arXiv:1909.07344 (2019).
  - [13] C. Bravo-Prieto, R. LaRose, M. Cerezo, Y. Subasi, L. Cincio, and P. J. Coles, arXiv preprint arXiv:1909.05820 (2019).
  - [14] A. Peruzzo, J. McClean, P. Shadbolt, M.-H. Yung, X.-Q. Zhou, P. J. Love, A. Aspuru-Guzik, and J. L. O’Brien, Nature Communications **5**, 4213 (2014).
  - [15] K. M. Nakanishi, K. Mitarai, and K. Fujii, Phys. Rev. Research **1**, 033062 (2019).
  - [16] R. M. Parrish, E. G. Hohenstein, P. L. McMahon, and T. J. Martínez, Phys. Rev. Lett. **122**, 230401 (2019).
  - [17] O. Higgott, D. Wang, and S. Brierley, Quantum **3**, 156 (2019).
  - [18] J. R. McClean, M. E. Kimchi-Schwartz, J. Carter, and W. A. de Jong, Phys. Rev. A **95**, 042308 (2017).
  - [19] P. J. Ollitrault, A. Kandala, C.-F. Chen, P. K. Barkoutsos, A. Mezzacapo, M. Pistoia, S. Sheldon, S. Woerner, J. Gambetta, and I. Tavernelli, Quantum equation of motion for computing molecular excitation energies on a noisy quantum processor (2019), arXiv:1910.12890.
  - [20] T. Jones, S. Endo, S. McArdle, X. Yuan, and S. C. Benjamin, Phys. Rev. A **99**, 062304 (2019).
  - [21] In this paper, we call  $|\langle \psi_1 | A | \psi_2 \rangle|^2$  a transition amplitude, rather than  $\langle \psi_1 | A | \psi_2 \rangle$ .
  - [22] J. J. Sakurai and J. Napolitano, *Modern Quantum Mechanics*, 2nd ed. (Cambridge University Press, 2017).
  - [23] N. J. Turro, V. Ramamurthy, V. Ramamurthy, and J. C. Scaiano, *Principles of molecular photochemistry: an introduction* (University science books, 2009).
  - [24] K. Mitarai and K. Fujii, Phys. Rev. Research **1**, 013006 (2019).
  - [25] H. Buhrman, R. Cleve, J. Watrous, and R. de Wolf, Phys. Rev. Lett. **87**, 167902 (2001).
  - [26] A. Kandala, A. Mezzacapo, K. Temme, M. Takita, M. Brink, J. M. Chow, and J. M. Gambetta, Nature **549**, 242 (2017).
  - [27] T. Jones, S. Endo, S. McArdle, X. Yuan, and S. C. Benjamin, Phys. Rev. A **99**, 062304 (2019).
  - [28] C. Hempel, C. Maier, J. Romero, J. McClean, T. Monz, H. Shen, P. Jurcevic, B. P. Lanyon, P. Love, R. Babbush, A. Aspuru-Guzik, R. Blatt, and C. F. Roos, Phys. Rev. X **8**, 031022 (2018).
  - [29] H. R. Grimsley, S. E. Economou, E. Barnes, and N. J. Mayhall, Nature Communications **10**, 10.1038/s41467-019-10988-2 (2019).

- [30] K. Hunger, *Industrial dyes: chemistry, properties, applications* (John Wiley & Sons, 2007).
- [31] P. K. Barkoutsos, J. F. Gonthier, I. Sokolov, N. Moll, G. Salis, A. Fuhrer, M. Ganzhorn, D. J. Egger, M. Troyer, A. Mezzacapo, S. Filipp, and I. Tavernelli, *Phys. Rev. A* **98**, 022322 (2018).
- [32] P. Virtanen, R. Gommers, T. E. Oliphant, M. Haberland, T. Reddy, D. Cournapeau, E. Burovski, P. Peterson, W. Weckesser, J. Bright, S. J. van der Walt, M. Brett, J. Wilson, K. J. Millman, N. Mayorov, A. R. J. Nelson, E. Jones, R. Kern, E. Larson, C. J. Carey, Í. Polat, Y. Feng, E. W. Moore, J. VanderPlas, D. Laxalde, J. Perktold, R. Cimrman, I. Henriksen, E. A. Quintero, C. R. Harris, A. M. Archibald, A. H. Ribeiro, F. Pedregosa, P. van Mulbregt, A. Vijaykumar, A. P. Bardelli, A. Rothberg, A. Hilboll, A. Kloeckner, A. Scopatz, A. Lee, A. Rokem, C. N. Woods, C. Fulton, C. Masson, C. Häggström, C. Fitzgerald, D. A. Nicholson, D. R. Hagen, D. V. Pasechnik, E. Olivetti, E. Martin, E. Wieser, F. Silva, F. Lenders, F. Wilhelm, G. Young, G. A. Price, G.-L. Ingold, G. E. Allen, G. R. Lee, H. Audren, I. Probst, J. P. Dietrich, J. Silterra, J. T. Webber, J. Slavič, J. Nothman, J. Buchner, J. Kulick, J. L. Schönberger, J. de Miranda Cardoso, J. Reimer, J. Harrington, J. L. C. Rodríguez, J. Nunez-Iglesias, J. Kuczynski, K. Tritz, M. Thoma, M. Newville, M. Kümmerer, M. Bolingbroke, M. Tartre, M. Pak, N. J. Smith, N. Nowaczyk, N. Shebanov, O. Pavlyk, P. A. Brodtkorb, P. Lee, R. T. McGibbon, R. Feldbauer, S. Lewis, S. Tygier, S. Sievert, S. Vigna, S. Peterson, S. More, T. Pudlik, T. Oshima, T. J. Pingel, T. P. Robitaille, T. Spura, T. R. Jones, T. Cera, T. Leslie, T. Zito, T. Krauss, U. Upadhyay, Y. O. Halchenko, Y. Vázquez-Baeza, and S. . . Contributors, *Nature Methods* 10.1038/s41592-019-0686-2 (2020).
- [33] Q. Sun, T. C. Berkelbach, N. S. Blunt, G. H. Booth, S. Guo, Z. Li, J. Liu, J. D. McClain, E. R. Sayfutyarova, S. Sharma, S. Wouters, and G. K. Chan, *Pyscf: the pythonbased simulations of chemistry framework* (2017), <https://onlinelibrary.wiley.com/doi/pdf/10.1002/wcms.1340>.
- [34] P. Jordan and E. Wigner, *Zeitschrift für Physik* **47**, 631 (1928).
- [35] I. G. Ryabinkin, S. N. Genin, and A. F. Izmaylov, *Journal of Chemical Theory and Computation* **15**, 249 (2018).
- [36] Qulacs, <https://github.com/qulacs>.
- [37] H.-J. Werner, P. J. Knowles, G. Knizia, F. R. Manby, M. Schütz, *et al.*, *Molpro*, version 2015.1, a package of ab initio programs (2015), see <https://www.molpro.net>.
- [38] C. Gonzalez and H. Schlegel, *The Journal of Chemical Physics* **90**, 2154 (1989).
- [39] J. T. Seeley, M. J. Richard, and P. J. Love, *The Journal of Chemical Physics* **137**, 224109 (2012).
- [40] S. Bravyi, J. M. Gambetta, A. Mezzacapo, and K. Temme, *Tapering off qubits to simulate fermionic hamiltonians* (2017), arXiv:1701.08213 [quant-ph].
- [41] H. Abraham, I. Y. Akhalwaya, G. Aleksandrowicz, T. Alexander, G. Alexandrowics, E. Arbel, A. Asfaw, C. Azaustre, AzizNgoueya, P. Barkoutsos, G. Barron, L. Bello, Y. Ben-Haim, D. Bevenius, L. S. Bishop, S. Bosch, S. Bravyi, D. Bucher, F. Cabrera, P. Calpin, L. Capelluto, J. Carballo, G. Carrascal, A. Chen, C.-F. Chen, R. Chen, J. M. Chow, C. Claus, C. Clauss, A. J. Cross, A. W. Cross, S. Cross, J. Cruz-Benito, C. Culver, A. D. Córcoles-Gonzales, S. Dague, T. E. Dandachi, M. Dartailh, DavideFrr, A. R. Davila, D. Ding, J. Doi, E. Drechsler, Drew, E. Dumitrescu, K. Dumon, I. Duran, K. EL-Safty, E. Eastman, P. Eendebak, D. Egger, M. Everitt, P. M. Fernández, A. H. Ferrera, A. Frisch, A. Fuhrer, M. GEORGE, J. Gacon, Gadi, B. G. Gago, J. M. Gambetta, A. Gammanpila, L. Garcia, S. Garton, J. Gomez-Mosquera, S. de la Puente González, I. Gould, D. Greenberg, D. Grinko, W. Guan, J. A. Gunnels, I. Haide, I. Hamamura, V. Havlicek, J. Hellmers, L. Herok, S. Hillmich, H. Horii, C. Howington, S. Hu, W. Hu, H. Imai, T. Imamichi, K. Ishizaki, R. Iten, T. Itoko, A. Javadi-Abhari, Jessica, K. Johns, T. Kachmann, N. Kanazawa, Kang-Bae, A. Karazeev, P. Kassebaum, S. King, Knabberjoe, A. Kovyrshin, V. Krishnan, K. Krsulich, G. Kus, R. LaRose, R. Lambert, J. Latone, S. Lawrence, D. Liu, P. Liu, Y. Maeng, A. Malyshev, J. Marecek, M. Marques, D. Mathews, A. Matsuo, D. T. McClure, C. McGarry, D. McKay, S. Meesala, M. Mevissen, A. Mezzacapo, R. Midha, Z. Minev, N. Moll, M. D. Mooring, R. Morales, N. Moran, P. Murali, J. Müggenburg, D. Nadlinger, G. Nannicini, P. Nation, Y. Naveh, P. Neuweiler, P. Niroula, H. Norlen, L. J. O’Riordan, O. Ogunbayo, P. Ollitrault, S. Oud, D. Padilha, H. Paik, S. Perriello, A. Phan, M. Pistoia, A. Pozas-iKerstjens, V. Prutyay, D. Puzzuoli, J. Pérez, Quintiii, R. Raymond, R. M.-C. Redondo, M. Reuter, J. Rice, D. M. Rodríguez, M. Rossmannek, M. Ryu, T. SAPV, SamFerracin, M. Sandberg, N. Sathaye, B. Schmitt, C. Schnabel, Z. Schoenfeld, T. L. Scholten, E. Schoute, I. F. Sertage, K. Setia, N. Shammah, Y. Shi, A. Silva, A. Simonetto, N. Singstock, Y. Siraichi, I. Sitdikov, S. Sivarajah, M. B. Sletfjerd, J. A. Smolin, M. Soeken, I. O. Sokolov, D. Steenken, M. Stypulkoski, H. Takahashi, I. Tavernelli, C. Taylor, P. Taylour, S. Thomas, M. Tillet, M. Tod, E. de la Torre, K. Trubing, M. Treinish, TrishaPe, W. Turner, Y. Vaknin, C. R. Valcarce, F. Varchon, A. C. Vazquez, D. Vogt-Lee, C. Vuillot, J. Weaver, R. Wiczorek, J. A. Wildstrom, R. Wille, E. Winston, J. J. Woehr, S. Woerner, R. Woo, C. J. Wood, R. Wood, S. Wood, J. Wootton, D. Yeralin, R. Young, J. Yu, C. Zachow, L. Zdanski, C. Zoufal, Zoufal, azulhner, bcamorrison, brandhsn, chlorophyll zz, dime10, drholmie, elfrocampeador, faisaldebouni, faniz-zamarco, gruu, kanejess, klinvill, kurarr, lerongil, ma5x, merav aharoni, ordmoj, sethmerkel, strickroman, sumitpuri, tigerjack, toural, vvlpas, willhbang, yang.luh, and yotamvakninibm, *Qiskit: An open-source framework for quantum computing* (2019).
- [42] K. Mitarai, M. Negoro, M. Kitagawa, and K. Fujii, *Phys. Rev. A* **98**, 032309 (2018).
- [43] M. Schuld, V. Bergholm, C. Gogolin, J. Izaac, and N. Kiloran, *Phys. Rev. A* **99**, 032331 (2019).
- [44] J. C. Garcia-Escartin and P. Chamorro-Posada, *Phys. Rev. A* **87**, 052330 (2013).